The QCD critical point and transport coefficients from holographic Bayesian analysis

Joaquín Grefa,

with M. Hippert, R. Kunnawalkam Elayavalli, J. Noronha,
J. Noronha-Hostler, C. Ratti, I. Portillo, and R. Rougemont

February 11$^{\text{th}}$ - 17$^{\text{th}}$, 2024

2024 Winter Workshop on Nuclear Dynamics

Outline

Table of Contents

QCD Phase Diagram

We can explore the QCD phase diagram by changing $\sqrt{s}$ in relativistic heavy ion collisions

Many models predict a first order phase transition line with a critical point

Lattice QCD is the most reliable theoretical tool to study the QCD phase diagram.

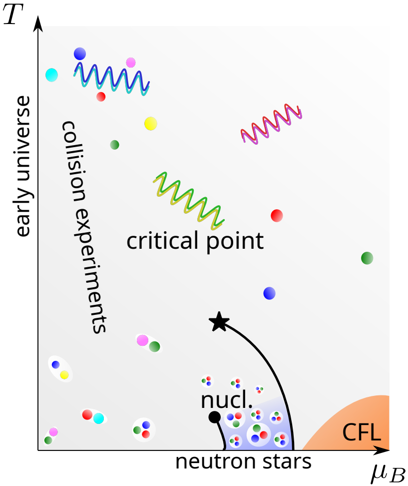

QCD Phase Diagram

We can explore the QCD phase diagram by changing $\sqrt{s}$ in relativistic heavy ion collisions

Many models predict a first order phase transition line with a critical point

Lattice QCD is the most reliable theoretical tool to study the QCD phase diagram.

Sign problem:

Equation of state for low to moderate μ_B/T.

Borsányi, Fodor, Guenther et al., PRL **126** (2021)

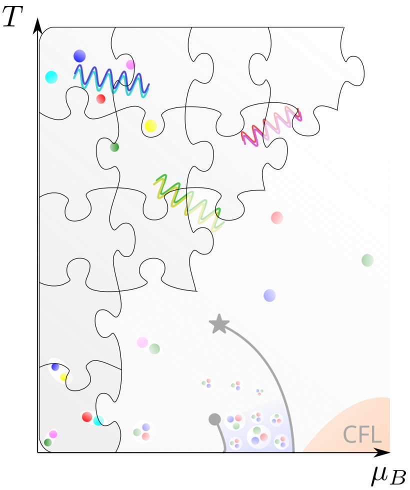

Model Requirements

Requirements:

-Deconfinement
-Nearly perfect fluidity
-Agreement with Lattice EoS at $\mu_B = 0$
-Agreement with baryon susceptibilities at $\mu_B = 0$

Taylor Expansion for small μ_B

$$\frac{P(T,\mu_B) - P(T,\mu_B = 0)}{T^4} =$$

$$\sum_{n=1}^{\infty} \frac{1}{(2n)!} \chi_{2n}(T) \left(\frac{\mu_B}{T}\right)^{2n}$$

where $\chi_n(T,\mu_B) = \frac{\partial^n (P/T^4)}{\partial(\mu_B/T)^n}$

- How can we fulfill these conditions?

Model Requirements

Requirements:

-Deconfinement
-Nearly perfect fluidity
-Agreement with Lattice EoS at $\mu_B = 0$
-Agreement with baryon susceptibilities at $\mu_B = 0$

Taylor Expansion for small μ_B

$$\frac{P(T,\mu_B) - P(T,\mu_B = 0)}{T^4} =$$

$$\sum_{n=1}^{\infty} \frac{1}{(2n)!} \chi_{2n}(T) \left(\frac{\mu_B}{T}\right)^{2n}$$

where $\quad \chi_n(T,\mu_B) = \frac{\partial^n (P/T^4)}{\partial(\mu_B/T)^n}$

- How can we fulfill these conditions?

HOLOGRAPHIC BLACK HOLES!!!

Table of Contents

Holography (Gauge/String duality)

Holographic gauge/gravity correspondence

5D Classical Gravity with asymptotically anti-de Sitter geometry $\Longleftrightarrow$ 3+1D Strongly coupled QFT in Minkowski spacetime

Maldacena 1997; Witten 1998; Gubser, Polyakov, Klebanov 1998

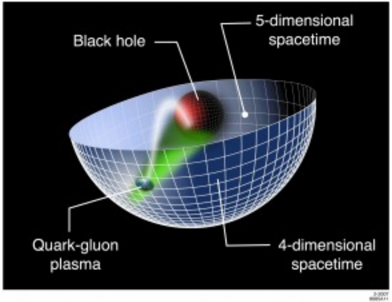

- Strongly coupled, nearly perfect fluid behavior of the QGP.

Kovtun, Son, Starinets. PRL 94 (2005)

Holography (Gauge/String duality)

Holographic gauge/gravity correspondence

5D Classical Gravity with asymptotically anti-de Sitter geometry	$\Longleftrightarrow$	3+1D Strongly coupled QFT in Minkowski spacetime

Maldacena 1997; Witten 1998; Gubser, Polyakov, Klebanov 1998

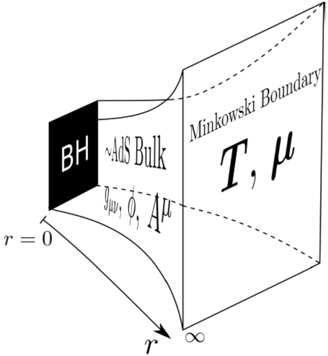

- Strongly coupled, nearly perfect fluid behavior of the QGP.

  Kovtun, Son, Starinets. PRL 94 (2005)

- BH solutions $\rightarrow$ QFT in T and μ.

Holography (Gauge/String duality)

Holographic gauge/gravity correspondence

5D Classical Gravity with asymptotically anti-de Sitter geometry $\Longleftrightarrow$ 3+1D Strongly coupled QFT in Minkowski spacetime

Maldacena 1997; Witten 1998; Gubser, Polyakov, Klebanov 1998

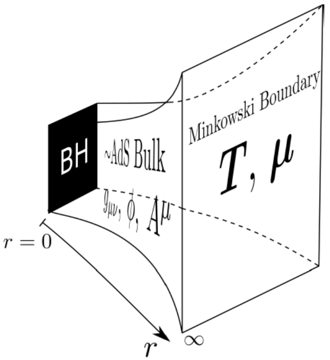

- Strongly coupled, nearly perfect fluid behavior of the QGP.

  Kovtun, Son, Starinets. PRL 94 (2005)

- BH solutions $\rightarrow$ QFT in T and μ.
- Can be constrained to mimic Lattice EoS at $\mu = 0$, and make predictions at finite density.

  J. G., et al. PRD 104 (2021)

Holography (Gauge/String duality)

Holographic gauge/gravity correspondence

5D Classical Gravity with asymptotically anti-de Sitter geometry $\Longleftrightarrow$ 3+1D Strongly coupled QFT in Minkowski spacetime

Maldacena 1997; Witten 1998; Gubser, Polyakov, Klebanov 1998

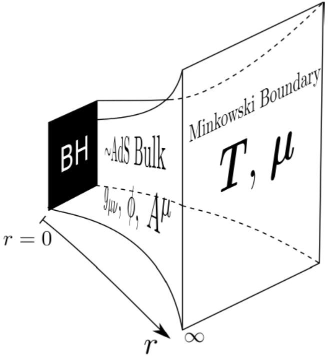

- Strongly coupled, nearly perfect fluid behavior of the QGP.

  Kovtun, Son, Starinets. PRL 94 (2005)

- BH solutions $\rightarrow$ QFT in T and μ.
- Can be constrained to mimic Lattice EoS at $\mu = 0$, and make predictions at finite density.

  J. G., et al. PRD 104 (2021)

- Able to handle near and out-of-equilibrium calculations.

  S. S. Gubser et al. PRL 101, (2008), J. G. et al. PRD 106 (2022)

O DeWolfe et al. Phys.Rev.D 83, (2011). R Rougemont et al. JHEP(2016)102. R. Critelli et al., Phys.Rev.D96(2017).

$$S = \frac{1}{2\kappa_5^2}\int_{M_5} d^5x\sqrt{-g}\left[R - \frac{(\partial_\mu\phi)^2}{2} - \underbrace{V(\phi)}_{\text{nonconformal}} - \underbrace{\frac{f(\phi)F_{\mu\nu}^2}{4}}_{\mu_B\neq 0}\right]$$

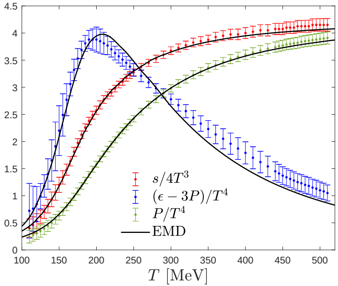

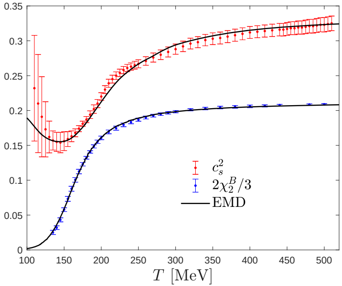

- Powerful, flexible model capable of describing crossover region and beyond.

S. S. Gubser and A. Nellore, PRD **78** (2008)
R. Critelli, J. Noronha, J. Noronha-Hostler, I. Portillo, C. Ratti, R. Rougemont, PRD **96** (2017)
J. Grefa, J. Noronha, J. Noronha-Hostler, I. Portillo, C. Ratti, R. Rougemont, PRD **104** (2021)

- Accurate prediction of χ_8 supported by lattice results.

R. Critelli, J. Noronha, J. Noronha-Hostler, I. Portillo, C. Ratti, R. Rougemont, PRD **96** (2017)
S. Borsanyi, Z. Fodor, J. N. Guenther, S. K. Katz, K. K. Szabo, A. Pasztor, I. Portillo and C. Ratti, JHEP **10** (2018)
R. Rougemont, R. Critelli and J. Noronha, PRD **98** (2018)

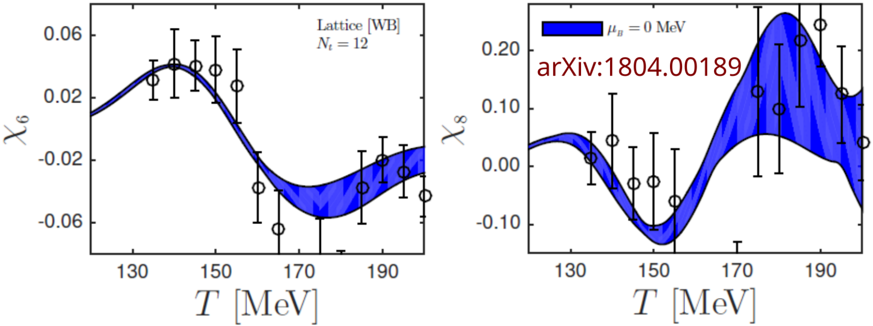

Polynomial-Hyperbolic Ansatz (PHA)

- Interpolates between arXiv:1706.00455 and arXiv:2201.02004

$$V(\phi) = -12\cosh(\gamma\,\phi) + b_2\,\phi^2 + b_4\,\phi^4 + b_6\,\phi^6$$

$$f(\phi) = \frac{\mathrm{sech}(c_1\phi + c_2\phi^2 + c_3\phi^3)}{1+d_1} + \frac{d_1}{1+d_1}\,\mathrm{sech}(d_2\phi)$$

Parametric Ansatz (PA)

- Similar shapes, more interpretable parameters ($\sim$ arXiv:1706.02647)

$$V(\phi) = -12\cosh\left[\left(\frac{\gamma_1\,\Delta\phi_V^2 + \gamma_2\,\phi^2}{\Delta\phi_V^2 + \phi^2}\right)\phi\right]$$

$$f(\phi) = 1 - (1 - A_1)\left[\frac{1}{2} + \frac{1}{2}\tanh\left(\frac{\phi - \phi_1}{\delta\phi_1}\right)\right] - A_1\left[\frac{1}{2} + \frac{1}{2}\tanh\left(\frac{\phi - \phi_2}{\delta\phi_2}\right)\right]$$

Mapping the QCD phase diagram from black hole solutions

The BH solutions are parametrized by (ϕ_0, Φ_1), where

$$\phi_0 \rightarrow \text{value of the scalar field at the horizon, and}$$

$$\Phi_1 \rightarrow \text{electric field in the radial direction at the horizon}$$

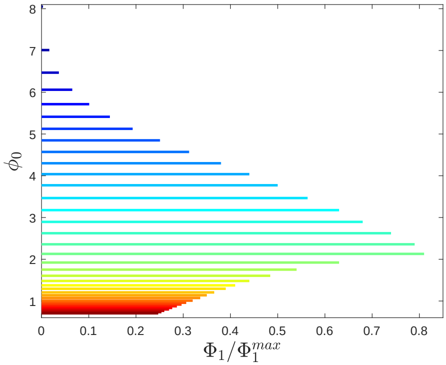

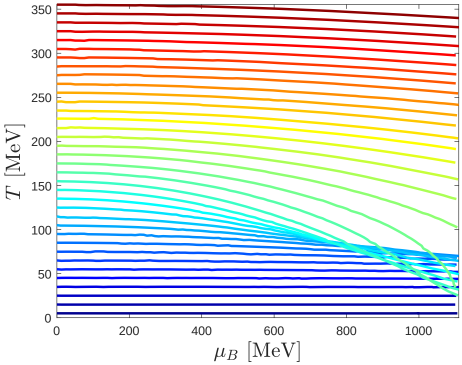

J. G et al. PRD.104 (2021)

Phase diagram

- Dilaton and electric fields at horizon: ϕ_0 and Φ_1 fully specify the physical state.
- Lines of constant ϕ_0 can cross.

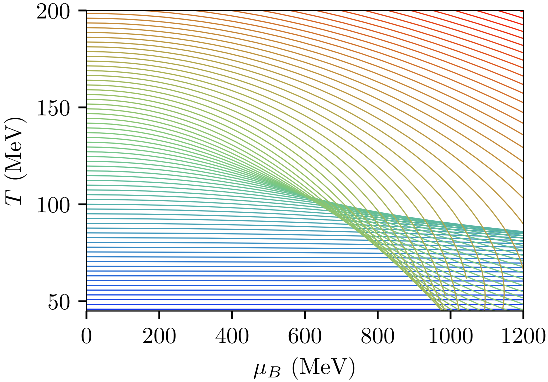

M. Hippert, J.G., T.A. Manning. J. Noronha, J. Noronha-Hostler, I. Portillo, C. Ratti, R. Rougemont, M. Trujillo, arXiv:2309.00579.

Phase diagram

- Dilaton and electric fields at horizon: ϕ_0 and Φ_1 fully specify the physical state.
- Lines of constant ϕ_0 can cross.
- Metastable states, spinodal lines.

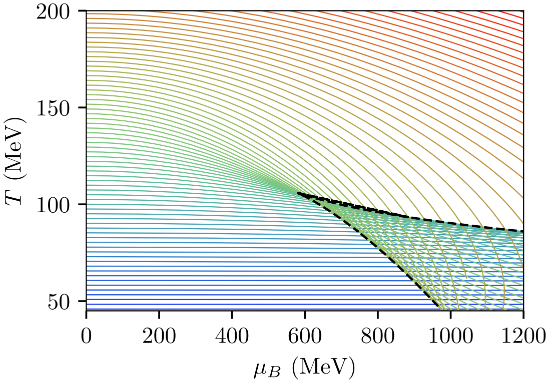

M. Hippert, J.G., T.A. Manning. J. Noronha, J. Noronha-Hostler, I. Portillo, C. Ratti, R. Rougemont, M. Trujillo, arXiv:2309.00579.

Phase diagram

- Dilaton and electric fields at horizon: ϕ_0 and Φ_1 fully specify the physical state.
- Lines of constant ϕ_0 can cross.
- Metastable states, spinodal lines.
- Critical point: where crossings start.
  Fast algorithm to find CP!

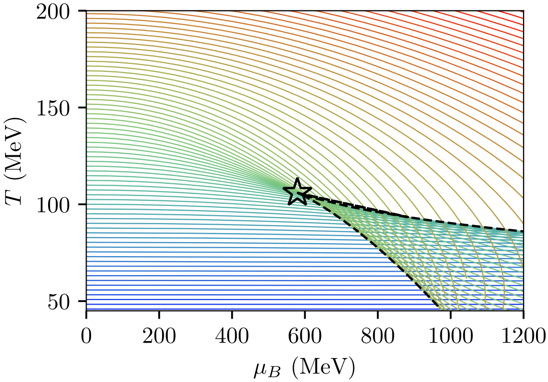

M. Hippert, J.G., T.A. Manning. J. Noronha, J. Noronha-Hostler, I. Portillo, C. Ratti, R. Rougemont, M. Trujillo, arXiv:2309.00579.

Phase diagram

- Dilaton and electric fields at horizon: ϕ_0 and Φ_1 fully specify the physical state.
- Lines of constant ϕ_0 can cross.
- Metastable states, spinodal lines.
- Critical point: where crossings start.
  Fast algorithm to find CP!
- Maxwell construction: first-order line.

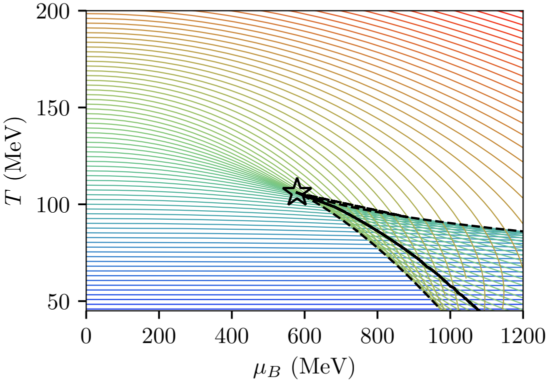

M. Hippert, J.G., T.A. Manning. J. Noronha, J. Noronha-Hostler, I. Portillo, C. Ratti, R. Rougemont, M. Trujillo, arXiv:2309.00579.

Table of Contents

Bayesian black-hole engineering

- How do lattice results constrain phase diagram/critical point?
- Systematic scan over possible extrapolations to higher densities.
- Bayesian black-hole engineering: what scenarios described by model compatible with the lattice results + error bars.

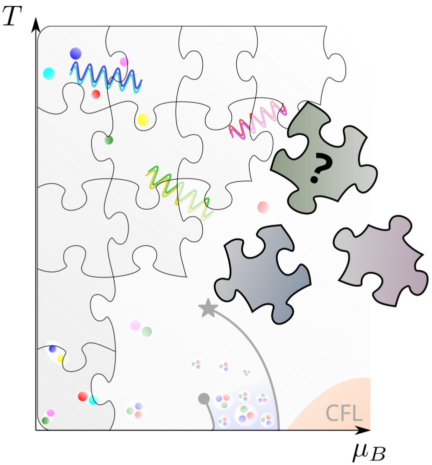

M. Hippert, J.G., T.A. Manning. J. Noronha, J. Noronha-Hostler, I. Portillo, C. Ratti, R. Rougemont, M. Trujillo, arXiv:2309.00579.

Assigning probabilities

Bayes' Theorem

$$\underbrace{P\left(\text{model}\,\middle|\,\text{results}\right)}_{\text{posterior } \mathcal{P}} \times P\left(\text{results}\right) = \underbrace{P\left(\text{results}\,\middle|\,\text{model}\right)}_{\text{likelihood } \mathcal{L}} \times \underbrace{P\left(\text{model}\right)}_{\text{prior knowledge}}$$

Gaussian Likelihood

$$\mathcal{L} = \exp\left\{-\frac{1}{2}\boldsymbol{\delta x}^T\boldsymbol{\Sigma}^{-1}\boldsymbol{\delta x} - \frac{1}{2}\log\det\boldsymbol{\Sigma} + \text{constant}\right\}$$

- $\boldsymbol{\delta x}$: deviation for $s(T)$ and $\chi_2^{(B)}(T)$ at $\mu = 0$.
- Correlation $\Gamma \equiv \exp\left(-\Delta T/\xi_T\right)$ between neighboring points $\rightarrow$ extra model parameter.

Markov Chain Monte-Carlo (MCMC)

- Start from prior (here, uniform).
- Random evolution to sample from posterior.
- Transition probabilities such that $\mathcal{P}$ is stationary limit.

C.J.F. Ter Braak, Statistics and Computing **16** (2006)

Metropolis-Hastings algorithm

1. Make small random changes to parameters.
2. Compute $\mathcal{P}$ from model EoS.
   - If $\mathcal{P}/\mathcal{P}_0 > 1$, transition to new parameters.
   - Otherwise, accept transition with probability $\mathcal{P}/\mathcal{P}_0$.
3. Repeat.

Markov Chain Monte-Carlo (MCMC)

- Start from prior (here, uniform).
- Random evolution to sample from posterior.
- Transition probabilities such that $\mathcal{P}$ is stationary limit.

C.J.F. Ter Braak, Statistics and Computing **16** (2006)

Metropolis-Hastings algorithm

1. Make small random changes to parameters.
2. Compute $\mathcal{P}$ from model EoS.
   - If $\mathcal{P}/\mathcal{P}_0 > 1$, transition to new parameters.
   - Otherwise, accept transition with probability $\mathcal{P}/\mathcal{P}_0$.
3. Repeat.

Inputs: Baryon susceptibility and entropy density from the lattice.

S. Borsanyi, Z. Fodor, C. Hoelbling, S. D. Katz, S. Krieg and K. K. Szabo, PRL **730** (2014)
Borsányi, Fodor, Guenther et al., PRL **126** (2021)

Table of Contents

Results

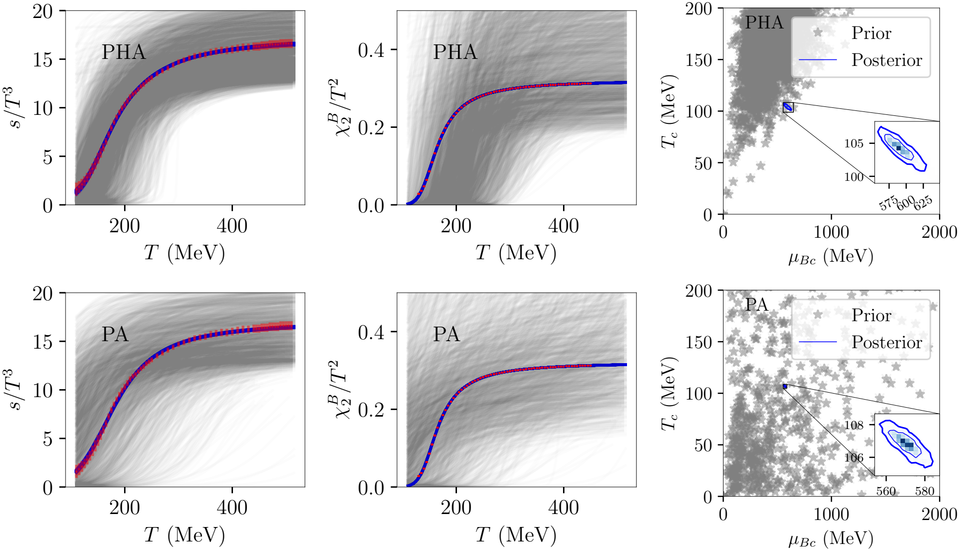

M. Hippert, J.G., T.A. Manning. J. Noronha, J. Noronha-Hostler, I. Portillo, C. Ratti, R. Rougemont, M. Trujillo, arXiv:2309.00579.

Posterior critical points

$(T_c,\, \mu_{Bc})_{PHA} = (104 \pm 3,\, 589^{+36}_{-26})$ MeV, $(T_c,\, \mu_{Bc})_{PA} = (107 \pm 1,\, 571 \pm 11)$ MeV.

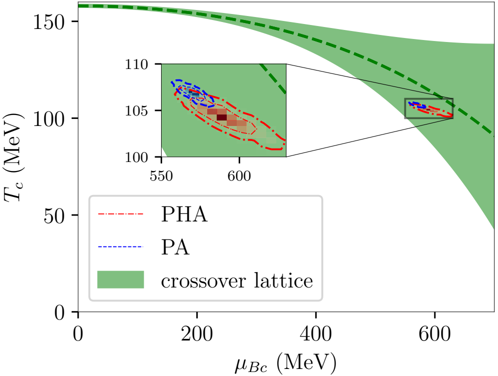

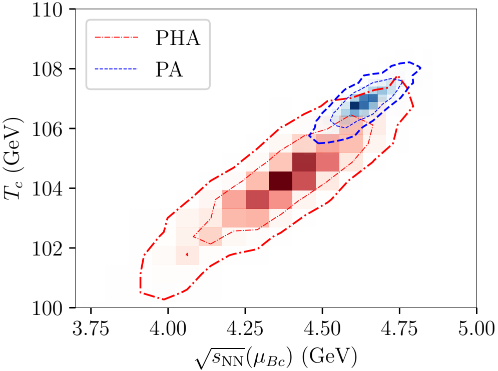

- Both Ansätze overlap at $1\,\sigma$. **Robust results!**

M. Hippert, J.G., T.A. Manning. J. Noronha, J. Noronha-Hostler, I. Portillo, C. Ratti, R. Rougemont, M. Trujillo, arXiv:2309.00579.

Table of Contents

Baryon Conductivity σ_B

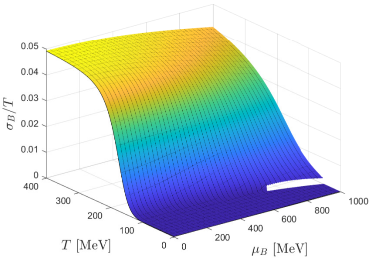

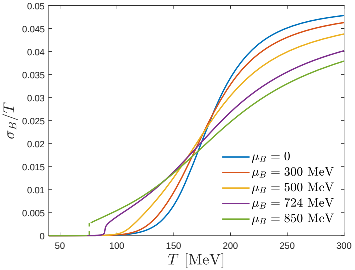

Can be computed from linear perturbations to the black hole background fields.

Overall dependence of σ_B/T with μ_B is relatively small.

σ_B/T remains finite at the critical point, and exhibits a discontinuity over the line of first order phase transition.

plots: J.G. et al. PRD.106 (2022)

Baryon Diffusion Coefficient

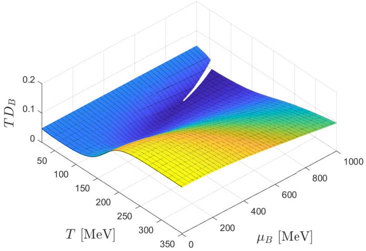

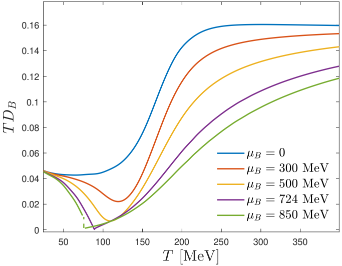

Nernst-Einstein Relation

$$D_B = \frac{\sigma_B}{\chi_2^B}$$

Controls the fluid response to inhomogeneities in the baryon density

The baryon diffusion charge is suppressed as the baryon chemical potential increases.

Vanishes at the location of the critical point.

plots: J.G. et al. PRD.106 (2022)

Holographic shear Viscosity

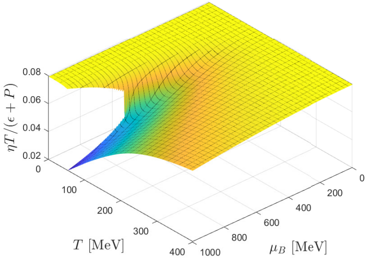

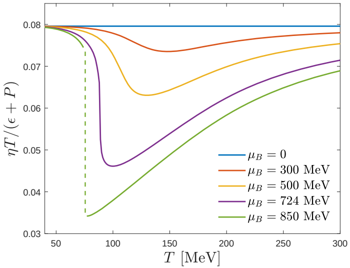

$\eta T/(\epsilon + P)$

measures the resistance to deformation in the presence of a velocity gradient in the layers of the fluid.

$$\frac{\eta T}{\epsilon + P} = \frac{1}{4\pi}\frac{1}{1+\frac{\mu_B \rho_B}{Ts}}$$

At $\mu_B = 0$, it reduces to the well known holographic result of $\eta/s = 1/4\pi$

plots: J.G. et al. PRD.106 (2022)

Bulk Viscosity

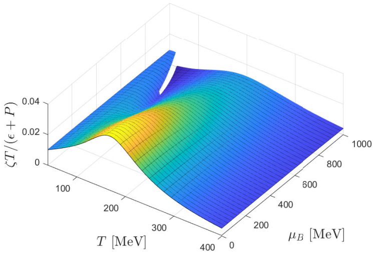

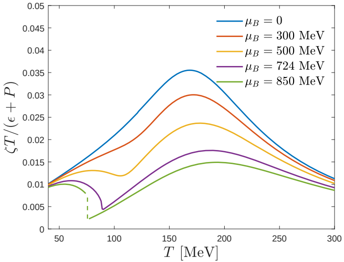

Measures the resistance to deformation of a fluid to a compression or expansion.

$$\frac{\zeta T}{\epsilon + p}(T, \mu_B) = \frac{\zeta}{s} \frac{1}{1 + \frac{\mu_B \rho_B}{T s}}$$

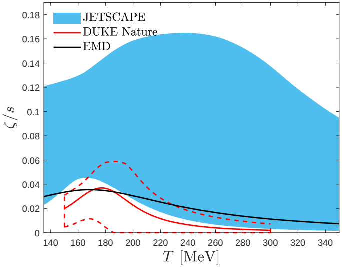

plots: J.G. et al. PRD.106 (2022)

Heavy quark Langevin Diffusion coefficient and jet quenching

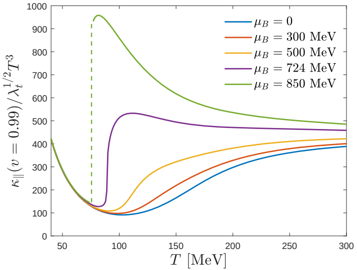

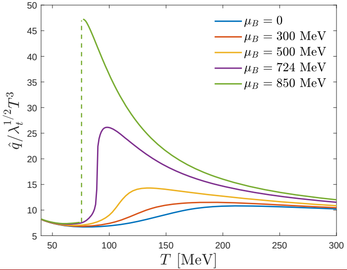

U. Gursoy et al. JHEP 0704 (2007)

Langevin diffusion coefficients

describe the thermal fluctuations of a heavy quark trajectory with constant velocity under Brownian motion.

F. D'Erano, H. Liu, K. Rajagopal. PRD 84 (2011)

The jet quenching parameter

characterizes the energy loss from collisional and radiative processes of high energy partons produced by the interaction with the hot and dense medium they travel through.

Their inflection point provides another way to characterize the crossover region.

plots: J.G. et al. PRD.106 (2022)

Jet energy loss modeling

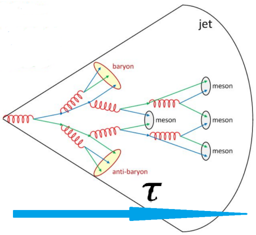

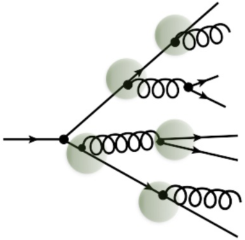

formation time

Time an emission takes to behave as an independent source of radiation.

$$\tau_{form} = \frac{1}{2Ez(1-z)(1-\cos\theta_{1,2})}$$

Energy and emission angle

taken from a distribution that depends on the jet quenching parameter $\hat{q}$

$$P(\theta,\omega) = \alpha\omega\theta^3\sqrt{\frac{2\omega}{\hat{q}}}L\exp\frac{-\theta^2\omega^2}{\sqrt{2\omega\hat{q}}}$$

L. Apolinario. Progress in Particle and Nuclear Physics, 103990

Translate T to τ

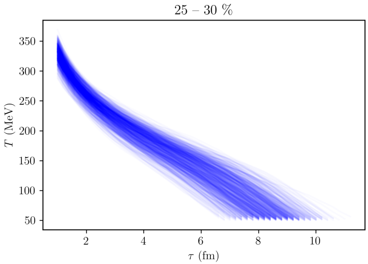

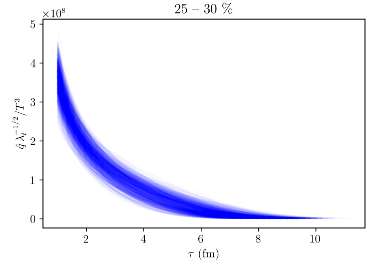

- TRENTo is used to model the initial state of relativistic heavy ion collisions.
- TRENTo provides a map of the energy density in the transverse plane (perpendicular to the collision axis) just after two heavy ions collide. Input: Holographic EoS.
- This energy density map is then evolved in time by using Bjorken hydrodynamics to model the QGP.

plots: J.G., Mauricio Hippert, et al (in preparation)

Translate T to τ

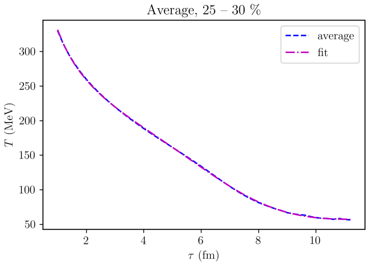

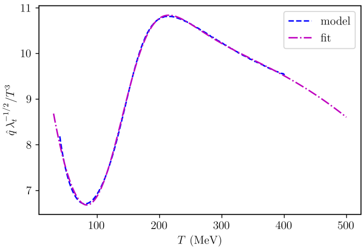

- TRENTo is used to model the initial state of relativistic heavy ion collisions.
- TRENTo provides a map of the energy density in the transverse plane (perpendicular to the collision axis) just after two heavy ions collide. Input: Holographic EoS.
- This energy density map is then evolved in time by using Bjorken hydrodynamics to model the QGP.
- The 't Hooft coupling (λ) should be fixed by phenomenological input.

plots: J.G., Mauricio Hippert, et al (in preparation)

Translate T to τ

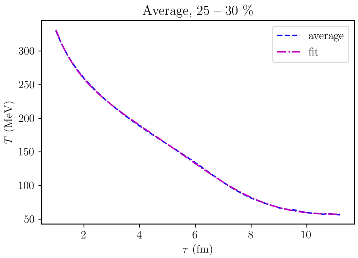

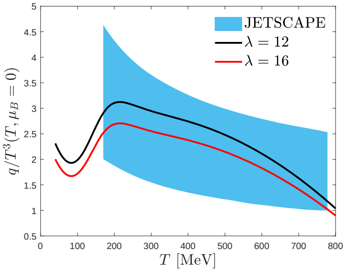

- TRENTo is used to model the initial state of relativistic heavy ion collisions.
- TRENTo provides a map of the energy density in the transverse plane (perpendicular to the collision axis) just after two heavy ions collide. Input: Holographic EoS.
- This energy density map is then evolved in time by using Bjorken hydrodynamics to model the QGP.
- The 't Hooft coupling (λ) should be fixed by phenomenological input.

plots: J.G., Mauricio Hippert, et al (in preparation)

JETSCAPE result: L. Apolinario. PPNP 103990

Preliminary results

Jets are less quenched as compared to a static $\hat{q}$. The overall degree of quenching of the jet population is reduced.

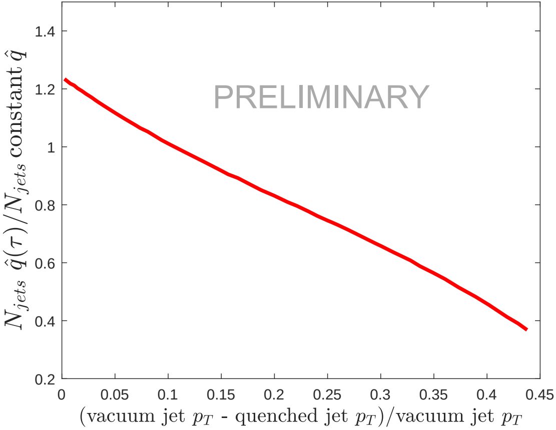

Table of Contents

Summary

1. Powerful description of the QGP, matching *finite-density* lattice results.

   J. Grefa, J. Noronha, J. Noronha-Hostler, I. Portillo, C. Ratti, R. Rougemont, PRD **104** (2021)
   J. Grefa, M. Hippert, J. Noronha, J. Noronha-Hostler, I. Portillo, C. Ratti and R. Rougemont, PRD **106** (2022)

2. Bayesian black-hole engineering: systematic exploration of phase diagram, informed by lattice QCD.

3. Critical point at $\mu_c \approx 560 - 625$ MeV, corresponding to $\sqrt{s} \approx 4.0 - 4.8$ GeV.

4. Larger statistical preference for a critical point after constraints:

   PA model: $\sim 20\%$ of prior $\Longrightarrow \sim 100\%$ of posterior.

   M. Hippert, J.G., T.A. Manning. J. Noronha, J. Noronha-Hostler, I. Portillo, C. Ratti, R. Rougemont, M. Trujillo, arXiv:2309.00579.

5. The holographic transport coefficients can be potentially used to model jet energy loss.

   J.G., Mauricio Hippert, et al (in preparation)

Towards a comprehensive EoS

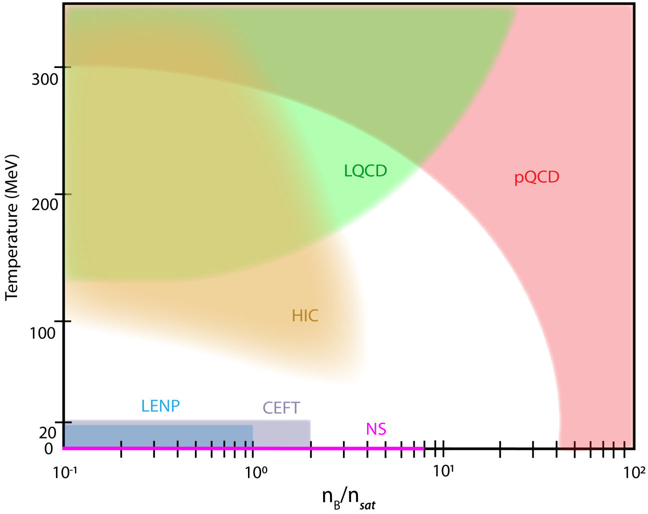

Towards a comprehensive EoS

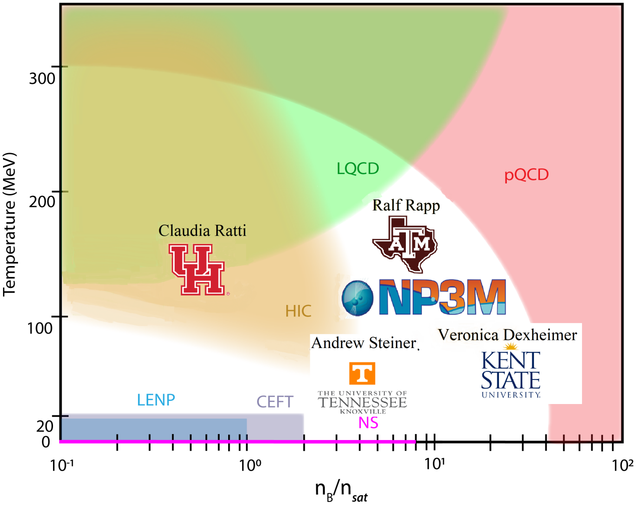

Appendix

Comparison with the state-of-the-art lattice QCD thermodynamics

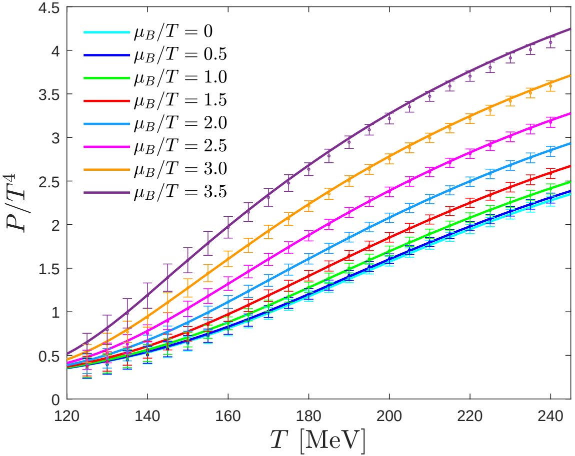

M. Hippert, J.G., T.A. Manning. J. Noronha, J. Noronha-Hostler, I. Portillo, C. Ratti, R. Rougemont, M. Trujillo, arXiv:2309.00579.

Comparison with the state-of-the-art lattice QCD thermodynamics

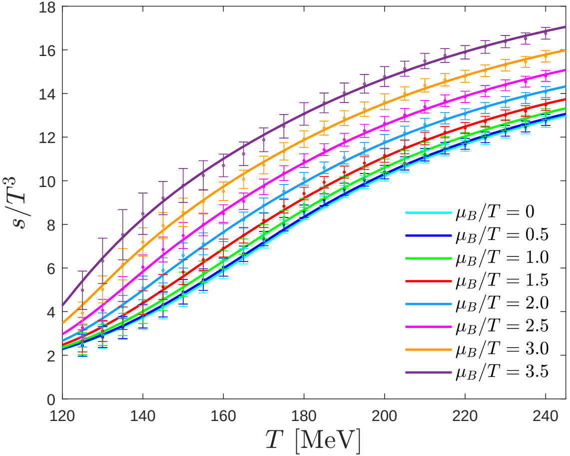

M. Hippert, J.G., T.A. Manning. J. Noronha, J. Noronha-Hostler, I. Portillo, C. Ratti, R. Rougemont, M. Trujillo, arXiv:2309.00579.

Holographic Phase Diagram

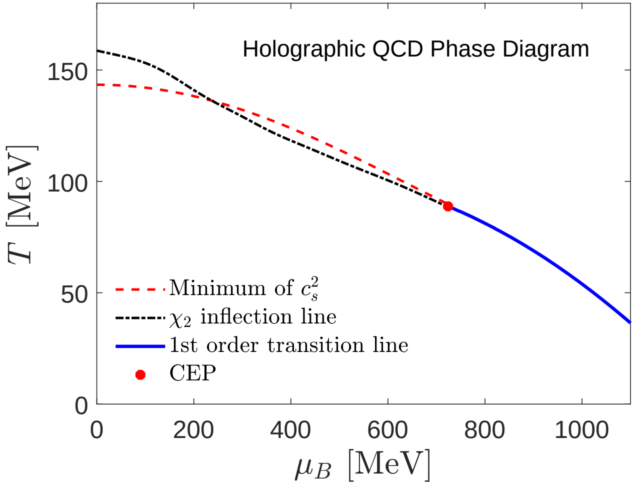

J. G et al. PRD.104 (2021)

Holographic Phase Diagram

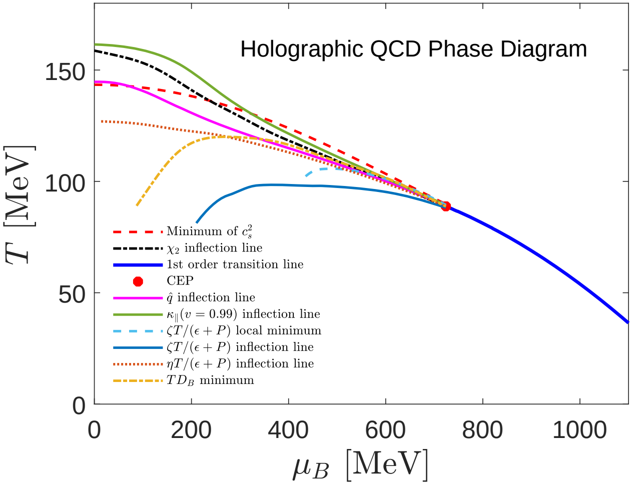

J.G. et al. PRD.106 (2022)

Locating the first order phase transition line

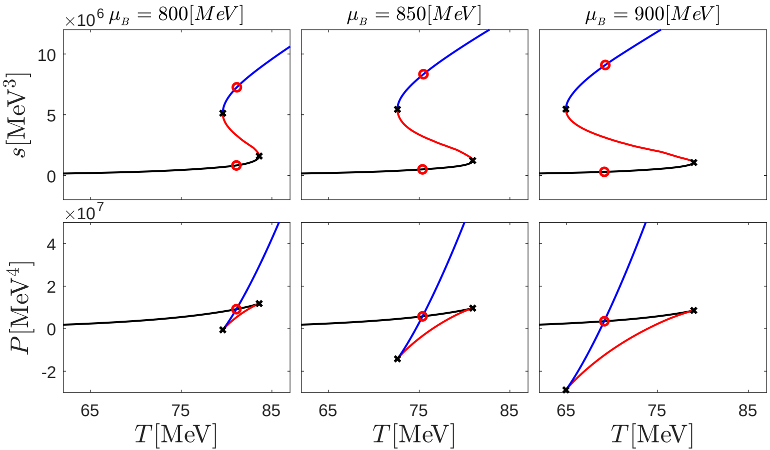

J. G et al. arXiv:2102.12042 [nucl-th].

Equations of Motion

$$S = \frac{1}{2\kappa_5^2}\int_{M_5} d^5x\sqrt{-g}\left[R - \frac{(\partial_\mu\phi)^2}{2} - \underbrace{V(\phi)}_{\text{nonconformal}} - \underbrace{\frac{f(\phi)F_{\mu\nu}^2}{4}}_{\mu_B\neq 0}\right]$$

$$ds^2 = e^{2A(r)}[-h(r)dt^2 + d\vec{x}^2] + \frac{e^{2B(r)}dr^2}{h(r)} \quad \phi = \phi(r) \quad A_\mu dx^\mu = \Phi(r)dt$$

Equations of Motion

$$\phi''(r) + \left[\frac{h'(r)}{h(r)} + 4A'(r)\right]\phi'(r) - \frac{1}{h(r)}\left[\frac{\partial V(\phi)}{\partial\phi} - \frac{e^{-2A(r)}\Phi'(r)^2}{2}\frac{\partial f(\phi)}{\partial\phi}\right] = 0$$

$$\Phi''(r) + \left[2A'(r) + \frac{d[\ln f(\phi)]}{d\phi}\phi'(r)\right]\Phi'(r) = 0$$

$$A''(r) + \frac{\phi'(r)^2}{6} = 0$$

$$h''(r) + 4A'(r)h'(r) - e^{-2A(r)}f(\phi)\Phi'(r)^2 = 0$$

$$h(r)[24A'(r)^2 - \phi'(r)^2] + 6A'(r)h'(r) + 2V(\phi) + e^{-2A(r)}f(\phi)\Phi'(r)^2 = 0$$

Solutions

Far-Region asymptotics:

$$A(r) = \alpha(r) + \mathcal{O}(e^{-2\nu\alpha(r)}), \qquad where\ \alpha(r) = A_{-1}^{far} r + A_0^{far}$$
$$h(r) = h_0^{far} + \mathcal{O}(e^{-4\alpha(r)}),$$
$$\phi(r) = \phi_A e^{-\nu\alpha(r)} + \mathcal{O}(e^{-(2+\nu)\alpha(r)}),$$
$$\Phi(r) = \Phi_0^{far} + \Phi_2^{far} e^{-1\alpha(r)} + \mathcal{O}(e^{-(2+\nu)\alpha(r)}),$$

Thermodynamics:

$$T = \frac{1}{4\pi\phi_A^{1/\nu}\sqrt{h_0^{far}}}\Lambda \qquad s = \frac{2\pi}{\kappa_5^2\phi_A^{3/\nu}}\Lambda^3$$

$$\mu_B = \frac{\Phi_0^{far}}{\phi_A^{1/\nu}\sqrt{h_0^{far}}}\Lambda \qquad \rho_B = -\frac{\Phi_2^{far}}{\kappa_5^2\phi_A^{3/\nu}\sqrt{h_0^{far}}}\Lambda^3$$

Baryon Conductivity

The EOM for the gauge invariant linearized vector perturbation $a(r, \omega)$ associated to the baryon conductivity is given by,

$$a'' + \left(2A' + \frac{h'}{h} + \frac{f'(\phi)}{f(\phi)}\phi'\right)a' + \frac{e^{-2A}}{h}\left(\frac{\omega^2}{h} - f(\phi)\Phi'^2\right)a = 0$$

which again must be solved with infalling wave condition at the horizon and normalized to unity at the boundary, what may be done by setting,

$$a(r, \omega) = \frac{r^{-i\omega} P(r, \omega)}{r_{max}^{-i\omega} P(r_{max}, \omega)}$$

The DC baryon conductivity in the EMD model is calculated by means of the following holographic Kubo formula,

$$\sigma_B(T, \mu_B) = -\frac{\Lambda}{2\kappa_5^2 \phi_A^{1/\nu}} \lim_{\omega \to 0} \frac{1}{\omega} \left(e^{2A} h f(\phi) Im[a * a']\right) [MeV]$$

Bulk Viscosity

The EOM for the gauge invariant linearized scalar perturbation $H(r,\omega)$ associated to the bulk viscosity is,

$$H'' + \left(4A' + \frac{h'}{h} + \frac{2\phi''}{\phi} - \frac{2A''}{A'}\right) H' +$$
$$\left[\frac{e^{-2A}\omega^2}{h^2} + \frac{h'}{h}\left(\frac{A''}{A'} - \frac{\phi''}{\phi'}\right) + \frac{e^{-2A}}{h\phi'}(3A'f'(\phi) - f(\phi)\phi')\Phi'^2\right] H = 0$$

which must be solved with infalling wave condition at the black hole horizon, and normalized to unity at the boundary, what may be done be setting,

$$H(r,\omega) = \frac{r^{-i\omega}F(r,\omega)}{r_{max}^{-i\omega}F(r_{max},\omega)}$$

The ratio between the bulk viscosity and the entropy density in the EMD model is then calculated by making use of the following holographic Kubo formula,

$$\frac{\zeta}{s}(T,\mu_B) = -\frac{1}{36\pi}\lim_{\omega\to 0}\frac{1}{\omega}\left(\frac{e^{4A}h\phi'^2 Im[H^*H']}{A'^2}\right)$$

Transport coefficients Formulas

$$\frac{F_{\text{drag}}}{\sqrt{\lambda_t}T^2}(T,\mu_B;v) = -8\pi v h_0^{\text{far}} e^{\sqrt{2/3}\phi(r_*)+2A(r_*)},$$

$$h(r_*) = h_0^{\text{far}} v^2$$

$$\frac{\kappa_{\parallel}}{\sqrt{\lambda_t}T^3}(T,\mu_B;v) = 16\pi v^3 (h_0^{\text{far}})^{5/2} \frac{e^{\sqrt{2/3}\phi(r_*)+3A(r_*)}}{h'(r_*)^2} \times$$
$$\times \left(h'(r_*)\left[4A'(r_*) + \sqrt{\tfrac{8}{3}}\phi'(r_*) + \frac{h'(r_*)}{h(r_*)}\right]\right)^{3/2},$$

$$\frac{\hat{q}}{\sqrt{\lambda_t}T^3}(T,\mu_B) = \frac{64\pi^2 h_0^{\text{far}}}{\int_{r_{\text{start}}}^{r_{\max}} dr \frac{e^{-\sqrt{2/3}\phi(r)-3A(r)}}{\sqrt{h(r)\left[h_0^{far}-h(r)\right]}}}$$

PHA model

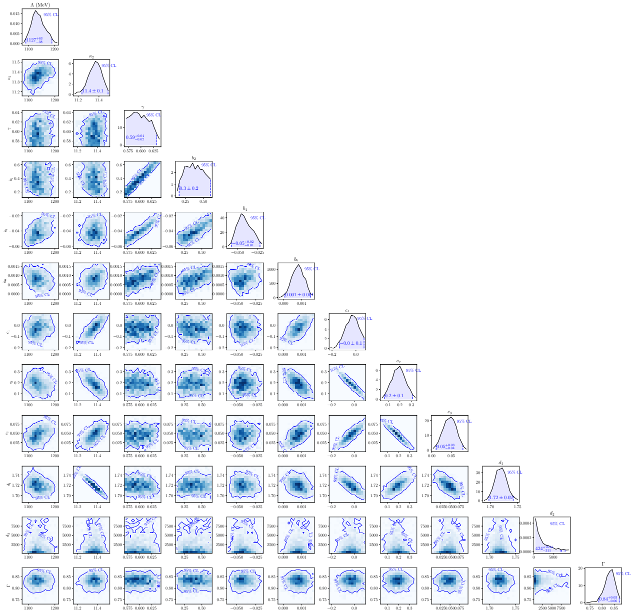
Λ (MeV)
1127^{+63}_{-38}
κ_2
11.4 ± 0.1
γ
$0.59^{+0.04}_{-0.02}$
b_2
0.3 ± 0.2
b_4
$-0.05^{+0.02}_{-0.01}$
b_6
0.001 ± 0.001
c_1
-0.0 ± 0.1
c_2
0.2 ± 0.1
c_3
$0.05^{+0.03}_{-0.04}$
d_1
1.72 ± 0.02
d_2
Γ
$0.84^{+0.03}_{-0.06}$
95% CL

PA model